Published in : *J. Phys. Chem. C* 2020, 124, 17, 9512-9522

https://doi.org/10.1021/acs.jpcc.0c00548

# Molecular Dynamics Simulations of Hydrated Poly(amidoamine) Dendrimer /Graphene-Oxide Nanocomposite Membranes

K. Steiakakis and K. Karatasos*

*Laboratory of Physical Chemistry, Department of Chemical Engineering, Aristotle University of Thessaloniki, 54124 Thessaloniki, Greece*

## Abstract

All atom molecular dynamics simulations were employed to explore graphene oxide/poly(amido amine)-dendrimer (GO/PAMAM) hydrated composite systems, as a function of temperature and dendrimer generation, at neutral pH conditions. Our main focus was to provide a detailed description regarding structural features in the microscopic level and to assess key-aspects related to the interfacial interactions related to the associative behavior between the two main components of the composites. It was found that the average separation between the GO sheets depended in a non-monotonical manner on the dendrimer generation. The structural coherence of the membranes increased as the size and the compactness of the dendrimer molecules increased. The dendrimers were found to physically adsorb on the GO surface. The GO/PAMAM association was driven by electrostatic interactions due to the development of a polar character in both components, as well as on hydrogen bonding involving charged groups. The latter was found to increase with temperature. Examination of the GO/PAMAM hydrogen-bonding dynamics revealed a temperature and generation independent mechanism which was persistent over the several-hundred-ns-wide trajectories examined in the simulations.

The detail afforded by the present study provides new insight towards the optimization of the performance of such membranes, based on a rational design at the microscopic level.

*Corresponding author: Tel.: +30-2310-995850; e-mail: karatas@eng.auth.gr (Kostas Karatasos)

## 1. Introduction

Polymer-based membranes are currently being used, or being considered for use, in a wide range of applications including uses in energy, e.g., in fuel cells and batteries[1-4], in environmental processes, e.g. as pollutant absorbents[5-8], and in other industrial applications such as in gas separation[9-10], water purification[11-12], desalination[13-14], etc. Despite the progress that has been made in their fabrication techniques and in their performance, general issues related to their structural stability, their resistance to degradation under prolonged operation and more specific issues such as their selectivity vs permeability or their responsiveness to external stimuli, are among those that need to be resolved for the improvement of their performance[15-16]. To this end, composite membranes comprised by polymeric and inorganic components (e.g, zeolites, carbon-based materials, ceramics etc) which can combine the desirable properties of the two components, show great potential in membrane development owing to their reliable processing strategies and their enhanced thermal and mechanical stability[17-19].

Recently, carbon-based composite materials have offered new routes for the fabrication of next-generation membranes with controlled structures and physicochemical properties[20-22]. Apart from the one-dimensional carbon nanotubes, progress on the synthesis and the processing protocols of two-dimensional graphene and its derivatives, offer new opportunities for the development of a novel class of membranes with exceptional properties[23-25]. In particular, graphene-based membranes fabricated following different approaches (e.g. drop-casting, vacuum filtration and spin-coating) possess favorable microstructures[23], responsiveness[22, 26-27] and distinct transport pathways, allowing them to be used for processes such as forward and reverse osmosis[26, 28], ultra- and nano-filtration[29-31], gas separation[10, 32], sensing[33-35], etc.

While in several of such applications, membranes based on pristine graphene appear as ideal candidates in cases where enhancement of conductivity or absorbance/filtration of organic compounds such as polycyclic aromatic hydrocarbons is desired, those based on its oxidized form, graphene oxide (GO), offer more facile means for their fabrication due to the liquid-phase processing feasibility (e.g, via well developed membrane-coating technology using GO dispersions) combined with a higher versatility in tuning their characteristics (e.g., their dispersibility, their selectivity and their anti-fouling properties) through chemical functionalization[31, 36-38]. In such GO-based membranes, adjustable

nanochannels between neighboring GO flakes can be formed allowing selective molecular or ionic transport[14, 22, 39]. The oxidized domains with, or without the presence of chemically attached molecules, can act as spacers to separate adjacent GO sheets and facilitate water intercalation, thus allowing high water-transport rates (which could promoted ionic conductivity[40-41]) while at the same time impeding permeation of other liquids, vapors and gases[42].

There are still many challenges related to the processing approaches for the fabrication of GO-based membranes with tunable characteristics, such as control of the inter-layer spacing after the hydration of GO in an aqueous environment[43] and achievement of an inter-locked microstructure which will ensure reproducibility in fabrication and structural stability[20-21, 44]. To address such challenges, a deeper understanding of the microscopic processes which are ultimately responsible for the structure-performance relationship becomes necessary. In this context, molecular simulations which can provide information down to the atomic level, is a unique tool towards this goal[45-46]. The benefits of employing fully atomistic molecular dynamics (MD) simulations to explore in detail morphological, mechanical, dynamic and thermodynamic properties of graphene-based polymeric membranes, have recently been demonstrated[46-51].

In this work we focus on hydrated graphene oxide/poly(amidoamine) dendrimer composites, exploring the effects of the size of the dendrimer molecules and of the temperature in structural and thermodynamic properties of the membranes. Poly(amido amine) (PAMAM) dendrimers are highly-branched polymers with a regular branching pattern, which starts from a focal point and emanates radially outward forming the so-called “generational shells” (see figure 1). The maximum number of such generational shells defines the generation number of the dendrimer. The high number of surface groups endows these molecules with high functionality, while their solubility in water and their nanoscale dimensions render them good candidates for the formation of GO-based composite membranes. In particular, their ability to ionize through protonation of their primary and tertiary amines depending on pH[52] essentially allows the control of their size (due to the electrostatic repulsion between the charged groups) and thus the morphological characteristics of their dispersion in aqueous GO solutions. Based on these attributes, recent experimental studies have explored the ability of GO/PAMAM composite membranes to act as materials for nanofiltration and other environmental and sensing applications [6, 14, 38, 53-55,56].

Previous simulational efforts have only addressed issues related to the microstructure of dendrimer/graphite composites[57] and the ability of graphene/PAMAM mixtures to bind aromatic contaminants from water[6]. Other computational works have addressed issues related to the enhancement of the dispersion of carbon-based fillers in the presence of PAMAM dendrimers[58-59]. In our study, the GO/PAMAM hydrated membranes will be examined at neutral pH levels, where both of the components appear in their ionized states as will be discussed in the section to follow.

## 2. Molecular Models and Simulation Protocol

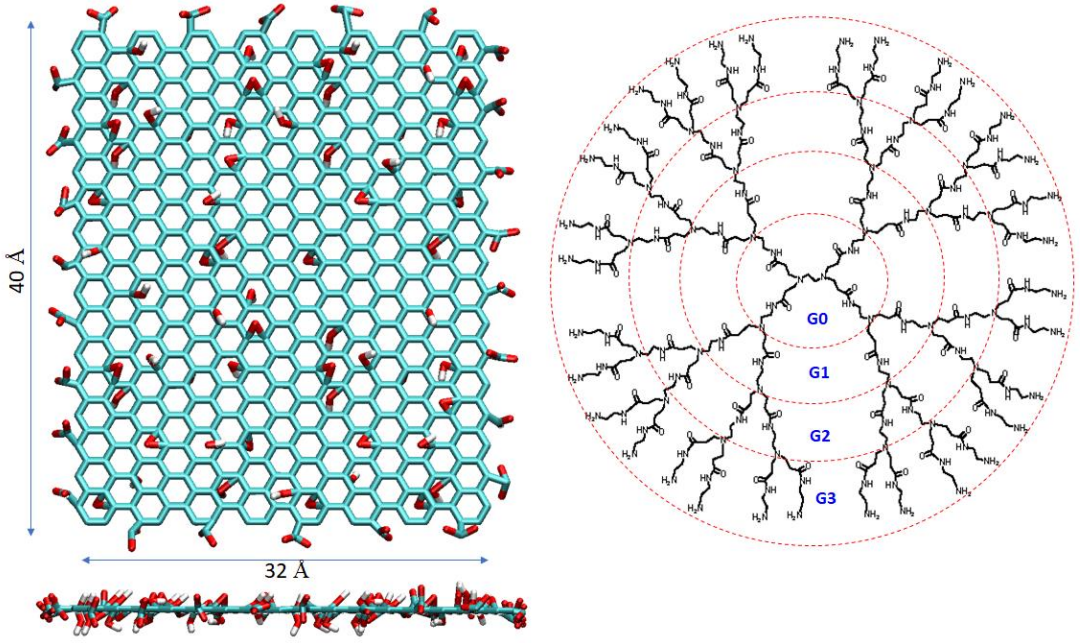


**Figure 1**: Schematic of a GO flake in frontal and lateral view (left), and of a 4$^{th}$ generation PAMAM dendrimer (right), used in the present study. In the GO representation, carbon atoms are shown in dark cyan, oxygen atoms in red and hydrogen atoms in white. The dashed circles in the PAMAM picture denote the different generational shells.

Modelling of the GO flake was based on the Lerf-Klinowski[60] scheme, which suggests that the epoxy and hydroxyl groups are distributed randomly on both sides of the basal carbon plane, while the carboxyl groups are attached to the carbon atoms on the edge. The construction procedure resulted to 1 carboxyl group every 20 carbon atoms[61]. The carbon to oxygen ratio was kept approximately to 5:1 and that of the hydroxyl to epoxy groups to 3:2. In addition, to mimic neutral pH conditions, all the carboxyl groups were taken to be ionized while the hydroxyl groups were kept protonated[62]. Parameterization

of the bonded and non-bonded interactions for the GO atoms was based on the OPLS-AA forcefield[63], which has recently been used for the description of oxidized forms of graphene[61, 64-66].

Structures for the different generations of the PAMAM molecules were taken from previous work[67]. Under neutral pH conditions, the primary amines of the PAMAM molecules (see figure 1) become protonated, while the tertiary amines remain uncharged[52]. For consistency purposes, the dendrimer molecules were also parameterized according to the all atom OPLS forcefield, which has previously been utilized for their energetic description in simulational studies[6]. Water molecules were modelled according to the TIP3P model[68]. The electric neutrality of the systems was maintained by the inclusion of an appropriate number of counterions (here using negatively charged $Cl^-$). The water content was 35% w for all systems. Such hydration levels of GO-based membranes have recently been studied in permeability studies[21]. Table 1 shows the composition of the examined models.

**Table 1.** Compositions of the simulated systems.

| System | Charge per PAMAM/GO molecule | Number of GO flakes | Number of PAMAM molecules | Number of $Cl^-$ counterions | Number of water molecules |
|---|---|---|---|---|---|
| GOPAMAM2 (G2) | +16/-26 | 18 | 88 | 940 | 15266 |
| GOPAMAM3 (G3) | +32/-26 | 18 | 44 | 940 | 15266 |
| GOPAMAM4 (G4) | +64/-26 | 18 | 22 | 940 | 15266 |

The dimensions of the GO flakes were kept at the nanoscale in order to be comparable to the average size of the dendritic molecules (the radius of gyration at physiological pH levels was found to be close to 20 Å for the largest size dendrimers[69]). Nanosized dispersions based on graphene and graphene oxide have recently been fabricated and studied experimentally[70-72].

All initial configurations of the models were constructed using the Packmol program[73]. The simulations were performed following the isothermal-isobaric (NPT) ensemble, at a pressure of P=1bar and at 3 different temperatures, i.e., 300K, 325K and 350K. Ensuing their construction, the models were energy minimized and equilibrated utilizing NPT MD for about 400ns. After the equilibration, stabilization of energetic and structural parameters was reached, including total and partial energies, the overall density, the average size of the dendrimers and the spatial arrangement of the components. Ensuing the equilibration, production runs of at least 400ns were generated and analyzed.

The MD simulations were performed using periodic boundary conditions and a timestep of 1 fs. The r-RESPA algorithm was employed for the computation of the long-range interactions every 2fs, and the frame saving frequency was set to 10 ps (higher saving frequencies were also used for specific purposes).

Temperature control was performed using the Langevin algorithm with a damping coefficient of 5 $ps^{-1}$, while pressure was controlled via the Nose-Hoover Langevin piston method[74] with a piston period of 0.1 ps and a decay time of 0.05 ps. Electrostatic interactions were evaluated using the particle mesh Ewald scheme[75]. All simulations were performed with NAMD 2.12[76] with a distance cutoff of 12 Å for the non-bonded interactions. Post-analysis was performed by custom-made routines.

Figure 2 portrays snapshots of the equilibrated models at T=300K (see fig. S1 in ESI for the initial configurations).

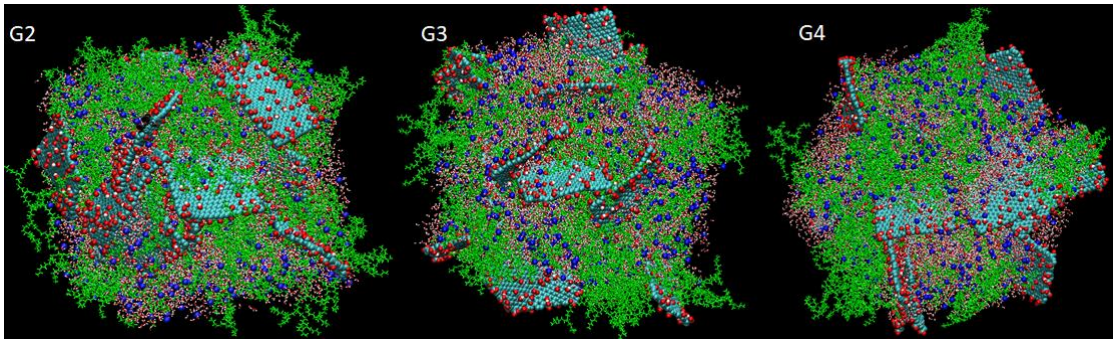


**Figure 2:** Equilibrated structures of the GOPAMAM2 (G2), GOPAMAM3(G3) and of the GOPAMAM4(G4) models at T=300K. Dendrimer molecules are shown in green, GO flakes as dark cyan (with red and white beads corresponding to the oxygen and the hydrogen atoms, respectively) and counterions in blue. Atoms of water molecules are shown as red (oxygen) and white (hydrogens) dots.

## 3. Results and discussion

### A. Conformational Characterization of the Dendritic Molecules in the Membranes

To characterize the conformational features of the dendritic molecules, we examined properties such as their size and their shape, as represented by their average radius of gyration ($R_g$)[67] and their asphericity[77]. As it was shown in previous studies of aqueous solutions of PAMAM dendrimers[67, 78], such features, apart from the dendrimer generation, they also depend on pH, while in the melt state they show a rather weak

temperature dependence[79]. Table 2 lists the radii of gyration of the dendrimers for the systems and at all the examined temperatures. Evidently, the average dimensions of the dendrimers are not sensitive in temperature at the examined range. Available literature data for the average $R_g$ of PAMAM dendrimers in aqueous solution at neutral pH conditions and at 300K, correspond to values of 13.6 Å, 17.2 Å and 21.7 Å for generations of 2,3 and 4 respectively[78]. Although for the size of the smallest generation there is a good agreement (see Table 2), the dimensions of the higher generation dendrimers in the composite systems examined here, appear to be smaller. This behavior might be related to the more constricted environment experienced by the dendrimers in the composites, which becomes more effective as the compactness of the dendritic structure increases when the generation grows[80-82].

**Table 2.** Radius of gyration, $R_{g,}$ of the dendrimers, in Å

| System | 300K | 325K | 350K |
|---|---|---|---|
| GOPAMAM2 (G2) | 13.66 ±0.03 | 13.73 ±0.03 | 13.77 ±0.04 |
| GOPAMAM3 (G3) | 15.13 ±0.04 | 15.48 ±0.08 | 15.51 ±0.05 |
| GOPAMAM4 (G4) | 16.97 ±0.05 | 17.40 ±0.10 | 17.70 ±0.07 |

Figure 3 shows the asphericity of the dendritic molecules as a function of dendrimer and generation. The closer the asphericity value to 0, the more spherically symmetric the distribution of the atoms with respect to the geometric center of the molecule.

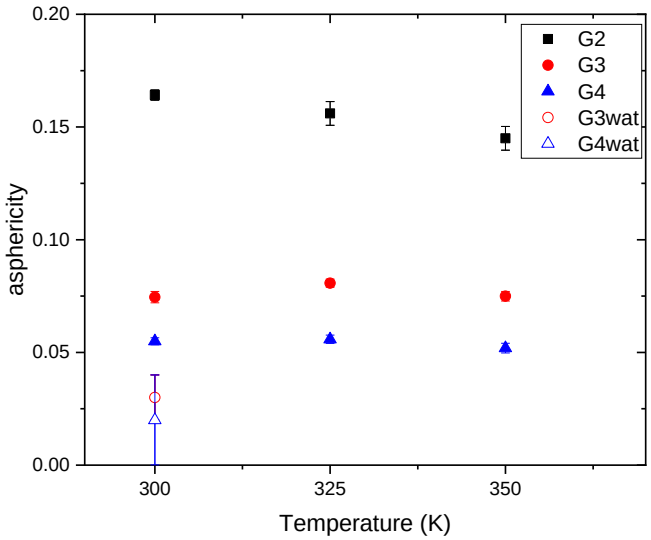


**Figure 3:** Asphericity of the dendrimer molecules in the GOPAMAM2 (G2), GOPAMAM3 (G3) and GOPAMAM4 (G4) systems. The open circle (G3wat) and the

triangle (G4wat) refer to literature asphericity data (see text) of PAMAM molecules in analogous GO-free systems, at T=300K.

Apart from the expected decrease of asphericity as the dendrimer generation grows[67, 82], it is also shown that the dendrimer shape in the composites practically remains unaffected by temperature in the examined range. This insensitivity in temperature characterizes also the internal structure of the dendrimers, as this was concluded by examining the density distributions with respect to their center of mass (see figure S2 in the SI). The asphericity of the G3 and the G4 dendrimers in a GO-free aqueous solution[67] at T=300K and at neutral pH conditions, was found to be 0.03±0.01 and 0.02±0.01 respectively, i.e., less than half compared to the corresponding values in the presence of GO. This indicates that the degree of deformation is the shape of the dendrimers is higher in the composite systems. A higher degree of shape anisotropy was also observed in PAMAM dendrimers in the presence of graphene, due to the physical adsorption of the dendrimers onto the graphene surface[83-84].

**B. Spatial arrangement of the components**

To assess the spatial arrangement of the components in the composite systems, we have calculated appropriate distribution functions, examining the relative positions between molecules of the same or different kind.

Figure 4 displays the radial distribution functions (rdf) arising from the center of mass of the GO sheets.

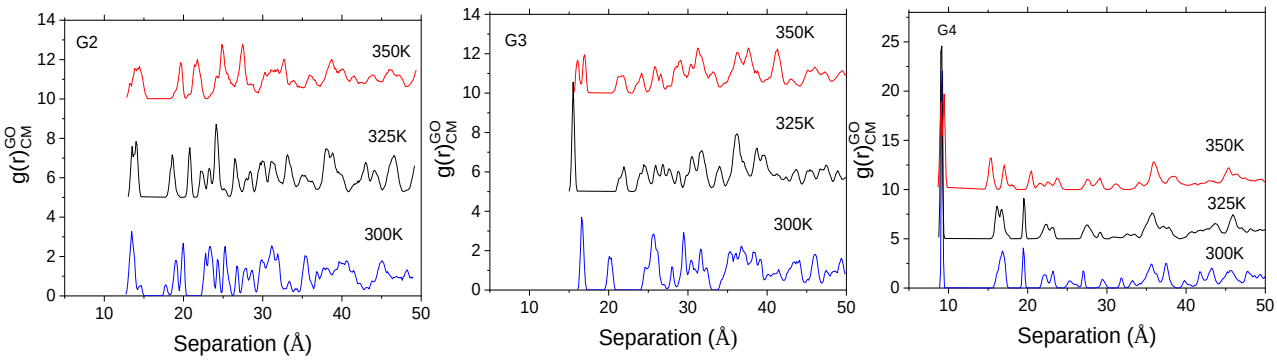


**Figure 4:** Radial distribution functions arising from the centers of mass of the GO flakes in the GOPAMAM2 (G2), the GOPAMAM3 (G3) and the GOPAMAM4(G4) models. The curves corresponding to 325K and 350K have been shifted in the y-axis by a value of 5 for clarity.

In all models and at all temperatures, the spectra are characterized by a multitude of sharp peaks and are reminiscent of those in semicrystalline materials[85]. Apparently, there are no significant differences between spectra of different temperatures at constant dendrimer generation. However, distinct features can be observed when comparing models at constant temperature but different dendrimer generation. Of particular interest are the spectral features (location, intensity, width) of the first peak, which corresponds to the closest neighbors. The location of the first maximum in the GOPAMAM2 model is close to 13 Å, for the GOPAMAM3 it is close to 16 Å and for the GOPAMAM4 it is close to 9 Å. These values are not far from interlayer GO distances close to 12 Å, observed experimentally[86-88] and computationally[89] in aqueous GO solutions under full hydration conditions, implying that multiple water layers have been interdigitated between the GO sheets[90]. The GO flakes in the presently examined systems, can be considered to be fully hydrated[89]. Therefore, the variation in the separation distance between the GO flakes denoted by the first peak in the respective rdf, should be attributed to the presence of dendrimers of different generation and the distinct characteristics of their spatial arrangement in the composites. It is also worth noting that both, the width and the intensity of the first-neighbor peak vary with generation. It is shown that as the size of the dendrimer grows, the width of the first maximum decreases while its intensity increases. Both of these features indicate that the localization of the GO within the composite becomes better as the dendrimer increases in generation, implying more stable structures.

To elaborate more on the characteristics of the dispersion of the PAMAM dendrimers and the GO in the membranes, it is also informative to examine the relative arrangement of one with respect to the other. Figure 5 portrays the density profiles of the GO nanosheets at T=325K, computed by considering spherical shells extending between r and r+dr (i.e., with width dr), where r is measured from the center of mass of a dendrimer.

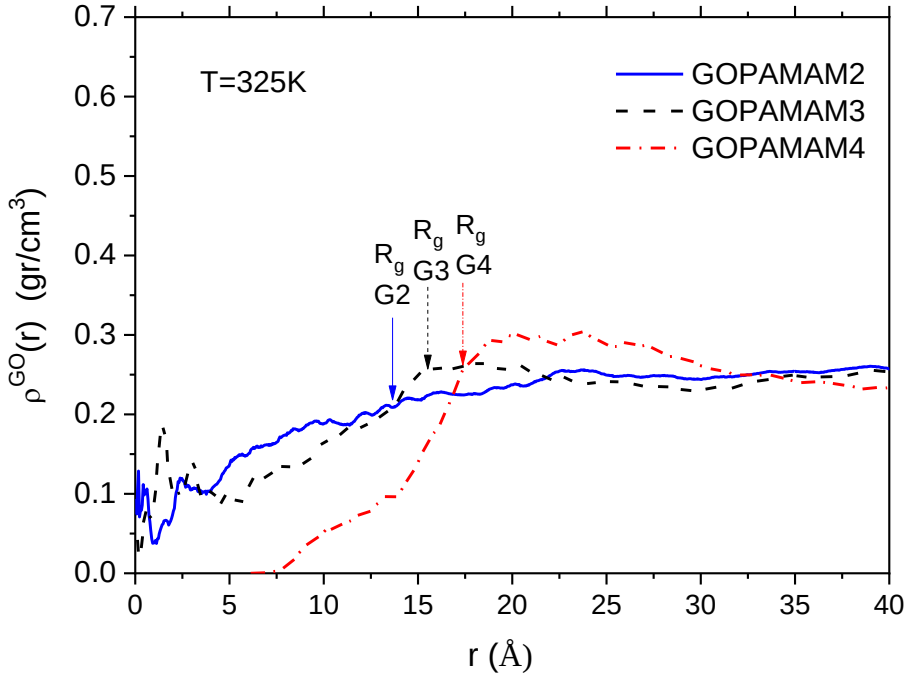


**Figure 5:** Radial distribution of the GO density at T=325K. The distance r is measured with respect to the center of mass of the dendritic molecules. The arrows denote the values of the radii of gyration of the different dendrimers in the composite membranes.

Visual inspection of fig. 5 shows that for the system with the lowest dendrimer generation, the GO density profile assumes values close to the long-distance limit even below the radius of gyration of the dendrimer. This indicates that GO atoms can be detected well within the dendritic structure. As the dendrimer generation grows, GO flakes become excluded from the dendritic interior while a broad maximum develops at distances close to the dendrimer periphery. This behavior is representative for all the temperatures examined (see figure S3 in the SI). The higher concentration of GO close to the dendrimer's surface as the generation grows, is consistent with the increase in the degree of localization of the GO sheets as inferred from the rdf spectra in figure 4.

Examination of the density distributions of the other components with respect to the center of mass of a dendrimer (see figure S4 in the SI), shows that water and $Cl^-$ ions can penetrate well with the dendritic interior. Figure 6 portrays the temperature and generation dependence of the percentage of Chlorine ions and water molecules which penetrate within the dendrimer's interior.

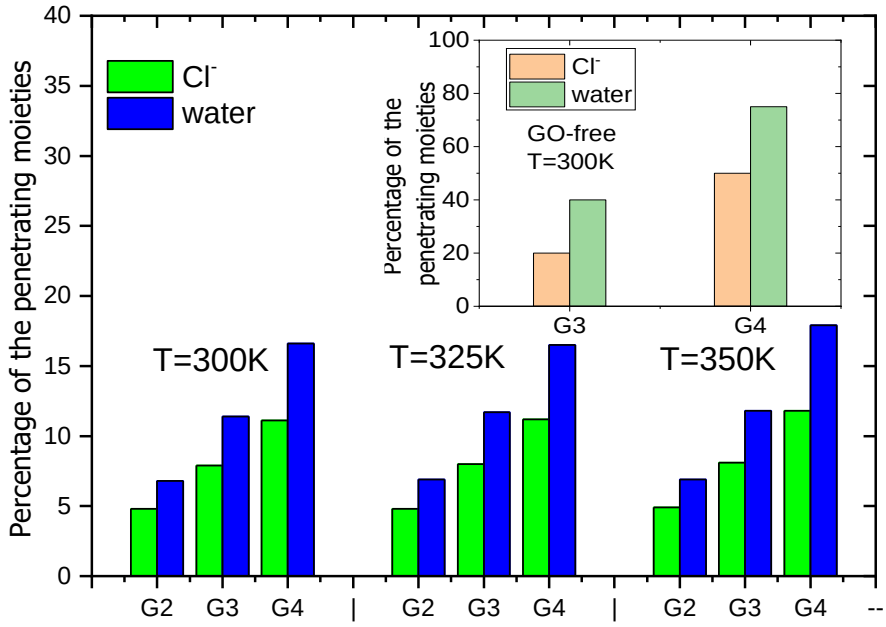


**Figure 6:** Percentage of $Cl^-$ ions and water molecules which penetrate within the dendritic molecules, in the GOPAMAM2 (G2), the GOPAMAM3 (G3) and the GOPAMAM4 (G4) models. The inset shows the same percentages in GO-free systems for PAMAM dendrimers of the 3rd (G3) and the 4th (G4) generation from ref. 67.

It appears that the percentage of the smaller moieties within the dendritic structure is insensitive in temperature in the examined range. However, it grows almost linearly with generation, despite that the dendritic volume increases much faster with size. This can be related to the well known backfolding effect observed in dendrimers[81, 91], which is enhanced as the generation of a dendrimer grows. It may also be related with the shrinkage of their volume (for the higher generations) compared to GO-free systems, as discussed in section 3A. A similar calculation for the percentage of the penetrating water molecules and the $Cl^-$ ions in GO-free systems (at T=300K) based on data from ref. [67] in dilute solution conditions, results to water percentages close to 20% and 50% and to $Cl^-$ percentages close to 40% and 75%, for the G3 and the G4 dendrimers, respectively. These differences emphasize the role of the constricted environment experienced by the dendrimers in the composite systems.

A complementary picture for the relative arrangement of the different components, can be obtained by calculating density profiles in a direction normal to the GO plane. The so-constructed density profiles with respect to the location of the GO plane, is shown in

figure 7, for the dendritic molecules. At distances close to GO, a sharp peak characterizes the curves of all systems and at all temperatures. The presence of this peak denotes a preferential accumulation of atoms belonging to dendrimers close to the GO surface, indicating a physical association between the two moieties. An additional common feature in the density profiles, is that the intensity of the first peak appears to be augmented as temperature increases. This behavior implies that a temperature-dependent mechanism related to the dendrimer/GO association, is at work. Moreover, a distinct feature between the density profiles characterizing the systems with different dendrimer generations, is the broad peak present at the GOPAMAM4 system. Its origin can be inferred, if one takes into account that it is centered at a distance close to the respective radius of gyration of the dendrimer. By combining this information with that emerging from figure 5, it appears that this broad peak can be ascribed to the relatively compact structure of the G4 dendrimers, immediately neighboring a GO flake. Figure S5 in the SI shows analogous profiles of all the constituents of the composite systems. It is shown that a higher concentration of water molecules and counterions is also present close to the GO plane, but with no marked dependence on the dendrimer generation and temperature. A higher concentration of counterions near the GO surface, could be driven by the presence of the dendrimers' protonated amines in the same vicinity. The increased concentration of water near the dendrimer/GO interface, is consistent with previous studies relevant to graphene/PAMAM dendrimer interactions[84], where it was found to play a significant role in the effective interaction between the two moieties.

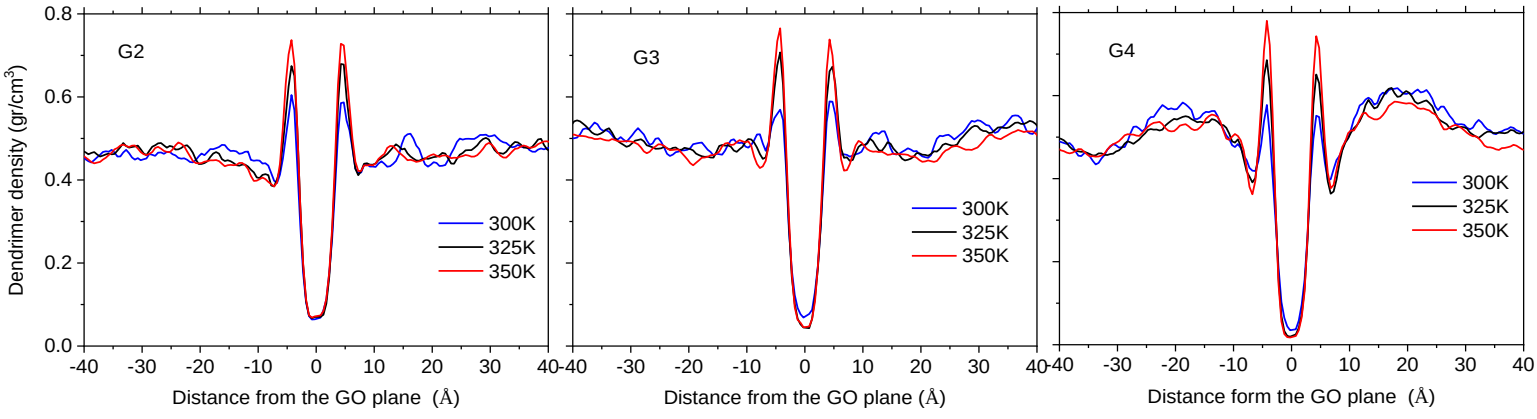


**Figure 7:** Density profiles of the dendrimer molecules in a direction normal to the GO plane, for the GOPAMAM2 (G2), the GOPAMAM3 (G3) and the GOPAMAM4 (G4) models. Distance 0 denotes the position of the GO plane. Positive and negative coordinates correspond to placements of the dendrimer from the one and the other side of the GO plane, respectively.

## C. Charge Distributions

Electrostatic interactions between the PAMAM dendrimers and GO, are among the main driving forces for the self-assembly and the stabilization of the formed structures[14]. To obtain information regarding the effective surface charge of the dendrimers and the GO molecules, we have monitored how the charge is distributed within the molecular structure and close to the molecular boundaries. Figure 8 illustrates the charge distribution within and close to the exterior of the PAMAM molecules. For the construction of the curves, charges from all the molecular species and the Chlorine counterions were taken into account. Visual inspection of figure 8 shows that charge distributions are insensitive to temperature in all models. In all systems a peak of positive charge is observed, at a distance from the center of mass, moderately larger compared to the corresponding radius of gyration. In the lower generation system, the effective charge fluctuates around 0 close to the dendrimer's boundary but also at longer distances. As the generation grows, a negative effective charge develops close to the dendrimer's periphery, which persists at longer distances from the center of mass. Table 3 displays the degree of neutralization of the initial charge of the dendrimer, from negative charges originating from the neighboring molecules and the $Cl^-$ ions (the effective dendrimer charge was calculated by integrating the distributions up to a dendrimer's boundary).

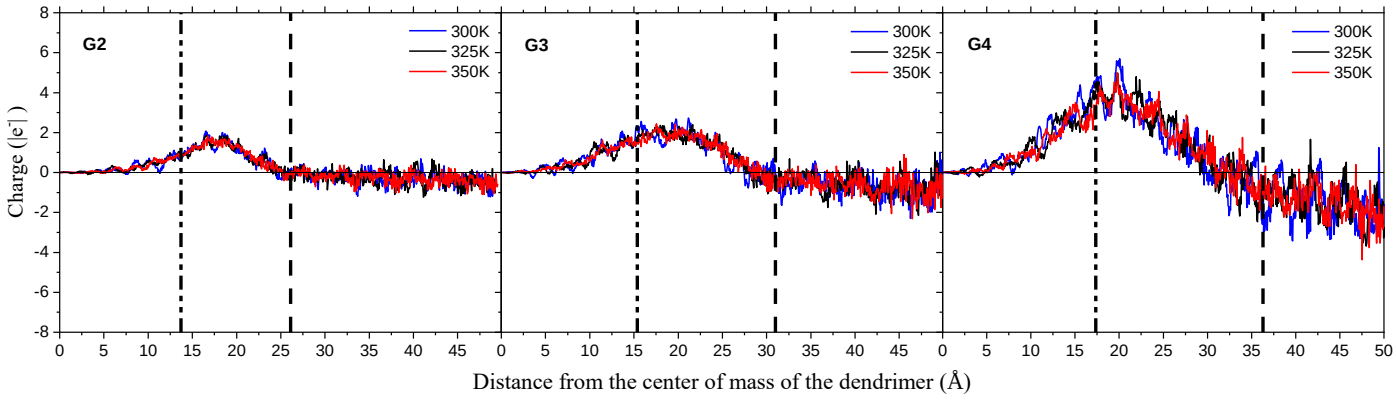


**Figure 8:** Radial overall-charge distributions (in units of the electron charge) with respect to the center of mass of the dendrimer molecules, for the GOPAMAM2 (G2), the GOPAMAM3 (G3) and the GOPAMAM4 (G4) models at all the temperatures examined. Dash-dot lines denote the location of the average radius of gyration for each dendrimer generation and dashed lines the boundary of the dendritic surface, as estimated through the corresponding density distributions (see fig S4 in the SI).

**Table 3.** Degree of dendrimer charge neutralization in the examined systems.

| System | Initial charge per dendrimer | Degree of neutralization | | |
|---|---|---|---|---|
| | | 300K | 325K | 350K |
| GOPAMAM2 | +16 | 3% | 4% | 4% |
| GOPAMAM3 | +32 | 14% | 15% | 14% |
| GOPAMAM4 | +64 | 17% | 17% | 18% |

The degree of neutralization is practically independent of temperature but appears to increase with generation. The origin for this behavior can be clarified if the contributions from the different components are examined separately (see figure S6 in SI). Quantification of the relative contributions of the negatively charged moieties to the degree of neutralization of the dendrimer charge, shows (see figure S7 in SI) that the contribution from the GO sheets increases as the dendrimer generation grows. This might be related to the fact that as the generation of a dendrimer increases, so does its surface and thus the number of GO sheets interacting with the dendrimer.

An analogous picture to that of figure 8 but from a reference frame centered on the GO flake, is shown in figure 9 at T=325K. The behavior at the other temperatures examined is similar (see fig. S8 in SI).

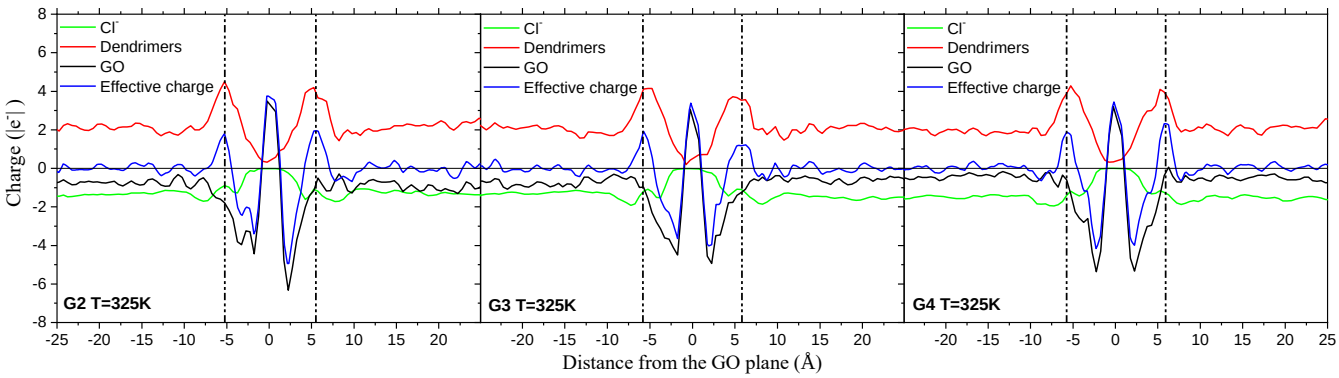


**Figure 9:** Charge distributions along a direction normal to the GO plane arising from the charged moieties at T=325K, for the GOPAMAM2 (G2), GOPAMAM3 (G3) and the GOPAMAM4 (G4) systems. The curve corresponding to the effective charge is the sum of the former distributions. The 0 value denotes the position of the GO sheet. The vertical dashed lines delimit the boundaries of a GO sheet, as follows from the location of the sharp peaks appearing in the corresponding density profiles in figure 7.

In all systems, the effective charge of the GO sheet variates in a characteristic manner. A positive peak at 0 distance, followed by a sharp negative peak at a distance close to 2.5Å and a positive maximum close to 5Å, on both sides of the GO flake. The positive peak at

distance 0 arises from the partial charges of the carbon atoms of GO, while the negative peak, originates mainly from charges of the carboxyl oxygens and the Chlorine counterions. The positive maxima in the effective charge, emanate from the adsorbed dendrimer molecules. According to this picture, GO sheets appear to develop a polar character which might prove beneficial as far as it concerns the electrical responsiveness of the composite membranes. It is also noteworthy, that the width of the charged layer ambilateral to the GO plane does not depend on the dendrimer generation; it rather relates to the nature of the interfacial interactions between the two moieties.

**D. Hydrogen Bonding**

Among the interfacial interactions in PAMAM/graphene oxide systems or in PAMAM composites with other carbon-based fillers, hydrogen bonding has been found to play a crucial role, which may affect drastically the dispersion characteristics and other physical properties of these materials[14, 58]. To detect the formation of hydrogen bonds between PAMAM dendrimers and GO sheets, we employed geometric criteria associated with the hydrogen–acceptor separation and with the angle formed by the donor–hydrogen–acceptor triplet. To this end, we examined appropriate hydrogen-acceptor pair distribution functions for those pairs forming donor–hydrogen–acceptor angles higher than 120 degrees[92]. A hydrogen bond was identified when the separation between such hydrogen-acceptor pairs, was smaller than the distance corresponding to the first minimum of the aforementioned distribution functions (see fig. S9 in the SI for examples of such pair distribution functions). The pairs we have examined, involved the hydrogens belonging to the protonated dendrimer amines and the three different kinds of oxygen atoms of the GO (i.e., oxygens belonging to the carboxyl , hydroxyl and epoxide groups). In all pairs examined, hydrogen bond formation was detected. However, the most abundant were those involving the oxygens of the negatively charged carboxyl groups of GO. Figure 10 illustrates the number of hydrogen bonds formed between the aforementioned dendrimer hydrogens and the carboxyl GO oxygens. Analogous histograms involving the other kinds of oxygen atoms of GO, are shown in figure S10 in the SI.

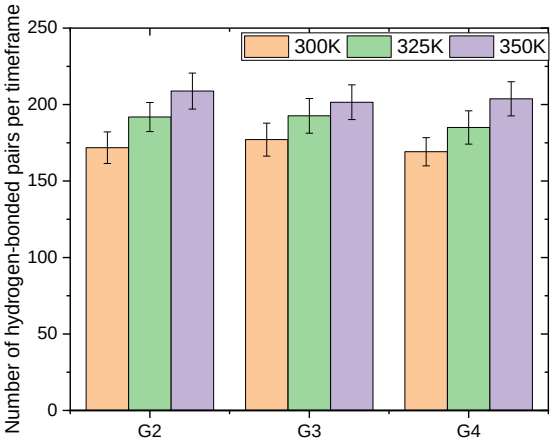


**Figure 10:** Average number of hydrogen bonds per saved timeframe, formed between the hydrogens of the protonated amine groups of the dendrimers and the carboxyl oxygens of GO, for the GOPAMAM2 (G2), GOPAMAM3 (G3) and the GOPAMAM4 (G4) models.

In all systems, the average number of hydrogen bonds at all temperatures (see also figure S10 in the SI), remains practically unaffected by the dendrimer generation. It does exhibit, however, a small increase with temperature. This observation is consistent with the behaviour described in figure 7, where the intensity of the dendrimer "adsorption" peak appeared also to increase with temperature. Therefore, a possible mechanism responsible for the latter effect, is that the increase in temperature provides the energy necessary for the local rearrangement of atoms close to the GO surface to take place, in a manner which favours more appropriate reorientations of the bonds involved in hydrogen bond formation.

An additional measure for the effectiveness of hydrogen bonding in enhancing the physical adsorption of the PAMAM molecules onto the GO surface, is their lifetime. Since hydrogen bond formation is a dynamic process[67, 93], the higher the longevity of the hydrogen bonds between the dendrimers and GO, the higher the affinity between the two components. To quantify this measure, appropriate hydrogen bond correlation functions[94] were calculated according to eq. 1:

$$h(t) = \frac{\langle g(t)\, g(0) \rangle}{\langle g^2 \rangle} \qquad (1)$$

Here, g(t) equals to 1 if the examined pair of atoms forms a hydrogen bond at time t, provided that these atoms were also hydrogen bonded at time t=0, and 0 otherwise. The averaging, as denoted by the angle brackets, was performed over all the examined pairs

and time origins. All the formation/breaking events between the time origin and time t are not taken into account. In this manner, h(t) essentially probes long time dynamics which is related to the probability of an initially hydrogen-bonded pair of atoms to remain at close enough distance and with the involved donor-hydrogen and hydrogen-acceptor bonds in appropriate orientations for hydrogen bonding, after time t.

Figure 11 shows h(t) correlation functions for the same pairs as those discussed in figure 10.

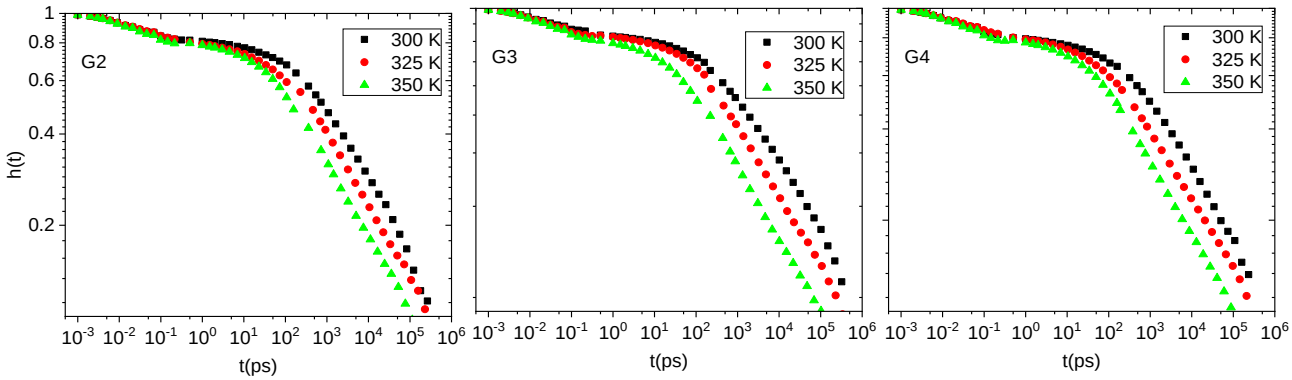


**Figure 11:** Hydrogen bonding correlation functions in log-log representation, between the hydrogens of the protonated amine groups of the dendrimers and the oxygens of the charged carboxyl groups of the GO sheets. G2:GOPAMAM2, G3:GOPAMAM3, G4:GOPAMAM4.

Visual inspection of the h(t) functions, shows that the systems with different dendrimer generations share common features. In all systems the correlation spectra appear to be described by 3 processes (note the two changes in slope near 0.1ps and between 10 and 100ps). The faster process can be assigned to the breaking/recombination of the hydrogen bonds, which arises from the rapid motion of hydrogen-bonded atoms around their equilibrium positions (i.e. involving a very short length scale), resulting in a transient violation or fulfillment of the geometric hydrogen-bonding criteria. The second process may arise from the wrinkling motion of GO[45, 95] which involves a characteristic timescale of the order of 10ps[45], that could also disrupt hydrogen bonds. The third and much slower process can be related to the main adsorption/desorption process between the dendritic polymers and GO[46, 48], involving a motion of larger in size parts of the dendrimer, such as the branch to which the hydrogen-bonded amine group is attached. The third, long-timescale mechanism is anticipated to play an important part to the tendency for association between the two components, and thus to important physical properties of such composites[37, 96-97].

Focusing on the temperature dependence of the h(t) spectra at constant dendrimer generation, it is clear that the main temperature effect emanates from the behavior of the slower process. At constant temperature, the dendrimer generation does not appear to affect the examined hydrogen-bonding dynamics (see figure S11 in the SI). To obtain information regarding the timescale associated with the probed h-bonding dynamics, we estimated the time it takes for the correlation function of eq. 1 to drop to 1/e, $\tau_{1/e}$. The so-calculated characteristic times, are plotted as a function of temperature in figure 12.

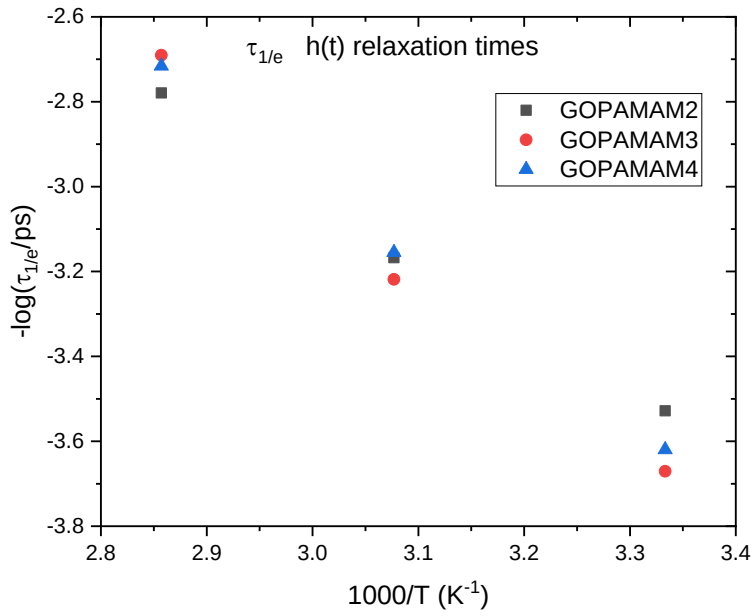


**Figure 12:** Activation plot of the $\tau_{1/e}$ times extracted from the correlation function shown in figure 11.

The disparities in characteristic times between systems with different dendrimer generations are rather small, as would be expected for processes involving short length scales which are insensitive to the overall polymer size. A simple linear fit to the data in figure 12, provides a first estimation regarding the activation energy related to the probed process. Taking into account the 3 different sets of points (see figure S12 in SI), the estimated activation energy varies between 3.1 and 4.1 kcal/mol, which lie within the range of values characterizing hydrogen bonds of typical strength[98-99].

## 4. Conclusions

In this work we have examined for the first time, through all-atom molecular dynamics simulations, hydrated PAMAM dendrimer/graphene oxide composite membranes. We aimed at exploring the effects of dendrimer generation and temperature on structural features of the dispersions, as well as on aspects related to the associative behaviour between the two main components. The systems were simulated under neutral pH and full hydration conditions for the GO flakes.

Compared to previous studies of PAMAM dendrimers in an GO-free aqueous environment, a moderate decrease in their size (particularly for the largest generation molecules) was observed; the degree of deformation in their shape was found to increase in the presence of GO, while it was not affected significantly by temperature in the composite systems, within the examined range. The spatial arrangement of the GO flakes was reminiscent of a semicrystalline solid, with the average separation between flakes depending on the dendrimer generation in an non-monotonical manner. The structural persistence of the GO dispersion in the membranes was found to increase with the dendrimer generation. This effect was attributed to the increasing compactness of the dendrimers upon an increase of generation. Based on this observation, it is expected that the structural persistence of such systems could be increased further, if higher generation dendrimers were employed.

Both of the main components of the composites (i.e., the PAMAM molecules and the GO flakes) were found to assume a polar character. For the dendrimer molecules, an effective negative charge close to their periphery was developed as the generation increased, while for the GO flakes a characteristic charge variation pattern was observed near their surface. Both of these features resulted (or triggered) mainly by their physical association, which brought in close proximity oppositely charged groups of the two moieties. The degree of dendrimer adsorption onto the GO surface increased moderately with temperature for all dendrimer generations. This was found to be related with an analogous increase in the degree of dendrimer/GO hydrogen bonding with temperature.

Hydrogen bonding between the two components was driven mainly by the formation of hydrogen bonds involving hydrogens (from the dendrimers) and oxygens (from the GO) belonging in the charged amine and carboxyl groups, respectively. This form of association between the two components, was found to be an activated process with a characteristic activation energy between 3 and 4 kcal/mol. Examination of the hydrogen bonding dynamics, showed that this interaction is relatively long-lived.

Previous work regarding the PAMAM/graphene association[84], showed that this was mainly driven by van der Waals (VDW) interactions and demonstrated the role of the dendrimer hydration near the graphene/dendrimer interface in this process. In the case of GO, where its increased nanorougness[45] (compared to pristine graphene) may work towards a decrease in the number of close atomic contacts at the interface (i.e., reducing the VDW interactions), hydrogen-bonding along with electrostatic forces[55] can act as strong associative factors which may assist the dispersion of GO and play a crucial role in an attempt to control key physical properties (mechanical, thermal, electrical) of such materials.

**Supporting Information:** Initial structures of the GOPAMAM2 (G2), GOPAMAM3(G3) and GOPAMAM4(G4) models, density distributions of the dendrimer molecules as a function of the distance from the center of mass of the dendritic structure, for the GOPAMAM2 (G2), the GOPAMAM3 (G3) and the GOPAMAM4 (G4) models, Density profiles of GO with respect to the center of mass of the dendritic molecules for the GOPAMAM2 (G2), the GOPAMAM3 (G3) and the GOPAMAM4 (G4) models, at all the examined temperatures, density profiles of all the components with respect to the center of mass of the dendritic molecules for the GOPAMAM2 (G2), the GOPAMAM3 (G3) and the GOPAMAM4 (G4) models at T=325K, density profiles of the different constituents of the composites, in a direction normal the GO plane, radial charge distributions arising from the different moieties, with respect to the center of mass of a dendrimer at T=325K, charge per GO sheet contributing to the neutralization of a dendrimer's positive charge, relative contribution of the negative charges arising from the GO flakes and the $Cl^-$ counterions to the neutralization of the charge of the PAMAM molecules at T=325K, charge distributions along a direction normal to the GO plane arising from the charged moieties, pair distribution functions of hydrogens belonging to the protonated primary amines of the dendrimers and oxygens belonging to the negatively charged hydroxyl groups of the GO, average number of hydrogen bonds per saved timeframe, formed between the hydrogens of the protonated amine groups of the dendrimers, hydrogen bonding correlations functions (eq. 1 in the main text) in log-log representation, between the hydrogens of the protonated amine groups of the dendrimers and the carboxyl oxygens of GO, linear fits through the data points referring to the systems with the 3 different dendrimer generations.

**Acknowledgements**

This work was supported by a computational time granted from the Greek Research & Technology Network (GRNET) in the National HPC facility - ARIS - under project ID DENDRIGO.

## References

1. Wang, X.; Lu, X.; Liu, B.; Chen, D.; Tong, Y.; Shen, G., Flexible Energy-Storage Devices: Design Consideration and Recent Progress. *Adv Mater* **2014**, *26*, 4763-82.
2. Vinothkannan, M.; Kim, A. R.; Gnana kumar, G.; Yoo, D. J., Sulfonated Graphene Oxide/Nafion Composite Membranes for High Temperature and Low Humidity Proton Exchange Membrane Fuel Cells. *RSC Adv.* **2018**, *8*, 7494-7508.
3. Mahmood, N.; Zhang, C.; Yin, H.; Hou, Y., Graphene-Based Nanocomposites for Energy Storage and Conversion in Lithium Batteries, Supercapacitors and Fuel Cells. *J. Mater. Chem. A* **2014**, *2*, 15-32.
4. Liu, W., et al., Ultrathin Dendrimer–Graphene Oxide Composite Film for Stable Cycling Lithium–Sulfur Batteries. *Proc. Natl. Acad. Sci.* **2017**, *114*, 3578-3583.
5. Huang, Y.; Zeng, M.; Ren, J.; Wang, J.; Fan, L.; Xu, Q., Preparation and Swelling Properties of Graphene Oxide/Poly(Acrylic Acid-Co-Acrylamide) Super-Absorbent Hydrogel Nanocomposites. *Colloids Surf. A* **2012**, *401*, 97-106.
6. DeFever, R. S.; Geitner, N. K.; Bhattacharya, P.; Ding, F.; Ke, P. C.; Sarupria, S., Pamam Dendrimers and Graphene: Materials for Removing Aromatic Contaminants from Water. *Environ. Sci. Technol.* **2015**, *49*, 4490-4497.
7. Zhang, F.; Wang, B.; He, S.; Man, R., Preparation of Graphene-Oxide/Polyamidoamine Dendrimers and Their Adsorption Properties toward Some Heavy Metal Ions. *J. Chem. Eng. Data* **2014**, *59*, 1719-1726.
8. Ju, X.-J.; Zhang, S.-B.; Zhou, M.-Y.; Xie, R.; Yang, L.; Chu, L.-Y., Novel Heavy-Metal Adsorption Material: Ion-Recognition P(Nipam-Co-Bcam) Hydrogels for Removal of Lead(Ii) Ions. *J. Hazard. Mater.* **2009**, *167*, 114-118.
9. v. Klitzing, R.; Tieke, B., Polyelectrolyte Membranes. In *Polyelectrolytes with Defined Molecular Architecture I*, Schmidt, M., Ed. Springer Berlin Heidelberg: Berlin, Heidelberg, 2004; pp 177-210.
10. Khakpay, A.; Rahmani, F.; Nouranian, S.; Scovazzo, P., Molecular Insights on the Ch4/Co2 Separation in Nanoporous Graphene and Graphene Oxide Separation Platforms: Adsorbents Versus Membranes. *J. Phys. Chem. C.* **2017**, *121*, 12308-12320.
11. Zhao, S.; Zou, L.; Tang, C. Y.; Mulcahy, D., Recent Developments in Forward Osmosis: Opportunities and Challenges. *J. Memb. Sci.* **2012**, *396*, 1-21.
12. Kamcev, J.; Galizia, M.; Benedetti, F. M.; Jang, E.-S.; Paul, D. R.; Freeman, B. D.; Manning, G. S., Partitioning of Mobile Ions between Ion Exchange Polymers and Aqueous Salt Solutions: Importance of Counter-Ion Condensation. *Phys. Chem. Chem. Phys.* **2016**, *18*, 6021-6031.
13. Homaeigohar, S.; Elbahri, M., Graphene Membranes for Water Desalination. *NPG Asia Mater.* **2017**, *9*, e427-e427.
14. Song, Y.; Li, R.; Pan, F.; He, Z.; Yang, H.; Li, Y.; Yang, L.; Wang, M.; Wang, H.; Jiang, Z., Ultrapermeable Graphene Oxide Membranes with Tunable Interlayer Distances Via Vein-Like Supramolecular Dendrimers. *J. Mater. Chem. A* **2019**, *7*, 18642-18652.
15. Baker, R. W., *Membrane Technology and Applications*; John Wiley & Sons, Ltd, 2012.
16. Park, H. B.; Kamcev, J.; Robeson, L. M.; Elimelech, M.; Freeman, B. D., Maximizing the Right Stuff: The Trade-Off between Membrane Permeability and Selectivity. *Science* **2017**, *356*, eaab0530.
17. Husain, S.; Koros, W. J., Mixed Matrix Hollow Fiber Membranes Made with Modified Hssz-13 Zeolite in Polyetherimide Polymer Matrix for Gas Separation. *J. Memb. Sci.* **2007**, *288*, 195-207.
18. Chau, M., et al., Composite Hydrogels with Tunable Anisotropic Morphologies and Mechanical Properties. *Chem. Mater.* **2016**, *28*, 3406-3415.

19. Kopeček, J.; Yang, J., Smart Self-Assembled Hybrid Hydrogel Biomaterials. *Angew. Chem. Int. Ed.* **2012**, *51*, 7396-7417.
20. Liu, G.; Jin, W.; Xu, N., Graphene-Based Membranes. *Chem. Soc. Rev.* **2015**, *44*, 5016-5030.
21. Thebo, K. H.; Qian, X.; Zhang, Q.; Chen, L.; Cheng, H.-M.; Ren, W., Highly Stable Graphene-Oxide-Based Membranes with Superior Permeability. *Nat. Commun.* **2018**, *9*, 1486-1486.
22. Ghaffar, A.; Zhang, L.; Zhu, X.; Chen, B., Scalable Graphene Oxide Membranes with Tunable Water Channels and Stability for Ion Rejection. *Environ. Sci. Nano* **2019**, *6*, 904-915.
23. Kral, P.; Titov, A. V.; Pearson, R., Sandwiched Graphene-Membrane Superstructures. *Acs Nano* **2010**, *4*, 229-234.
24. O'Neil, G. D.; Buiculescu, R.; Kounaves, S. P.; Chaniotakis, N. A., Carbon-Nanofiber-Based Nanocomposite Membrane as a Highly Stable Solid-State Junction for Reference Electrodes. *Anal Chem* **2011**, *83*, 5749-5753.
25. Sorokin, P. B.; Kvashnin, A. G.; Kvashnin, D. G., The Theoretical Study of Mechanical Properties of Graphene Membranes. *Fuller Nanotub Car N* **2010**, *18*, 497-500.
26. Nicolai, A.; Sumpter, B. G.; Meunier, V., Tunable Water Desalination across Graphene Oxide Framework Membranes. *Phys. Chem. Chem. Phys.* **2014**, *16*, 8646-8654.
27. Berke, B.; Czakkel, O.; Porcar, L.; Geissler, E.; Laszlo, K., Static and Dynamic Behaviour of Responsive Graphene Oxide-Poly(N-Isopropyl Acrylamide) Composite Gels. *Soft Matter* **2016**, *12*, 7166-7173.
28. Shao, F.; Dong, L.; Dong, H.; Zhang, Q.; Zhao, M.; Yu, L.; Pang, B.; Chen, Y., Graphene Oxide Modified Polyamide Reverse Osmosis Membranes with Enhanced Chlorine Resistance. *J. Memb. Sci.* **2017**, *525*, 9-17.
29. Qiu, L.; Zhang, X. H.; Yang, W. R.; Wang, Y. F.; Simon, G. P.; Li, D., Controllable Corrugation of Chemically Converted Graphene Sheets in Water and Potential Application for Nanofiltration. *Chem. Commun.* **2011**, *47*, 5810-5812.
30. Ling, S.; Qin, Z.; Huang, W.; Cao, S.; Kaplan, D. L.; Buehler, M. J., Design and Function of Biomimetic Multilayer Water Purification Membranes. *Sci. Adv.* **2017**, *3*, e1601939.
31. Lee, B.; Suh, D. W.; Hong, S. P.; Yoon, J., A Surface-Modified Edta-Reduced Graphene Oxide Membrane for Nanofiltration and Anti-Biofouling Prepared by Plasma Post-Treatment. *Environmental Science: Nano* **2019**, *6*, 2292-2298.
32. Dong, L.; Fan, W.; Tong, X.; Zhang, H.; Chen, M.; Zhao, Y., A Co2-Responsive Graphene Oxide/Polymer Composite Nanofiltration Membrane for Water Purification. *J. Mater. Chem. A* **2018**, *6*, 6785-6791.
33. Paek, K.; Yang, H.; Lee, J.; Park, J.; Kim, B. J., Efficient Colorimetric Ph Sensor Based on Responsive Polymer-Quantum Dot Integrated Graphene Oxide. *Acs Nano* **2014**, *8*, 2848-2856.
34. Zhang, H.; Gruner, G.; Zhao, Y., Recent Advancements of Graphene in Biomedicine. *J. Mater. Chem. B* **2013**.
35. Yang, K.; Feng, L.; Hong, H.; Cai, W.; Liu, Z., Preparation and Functionalization of Graphene Nanocomposites for Biomedical Applications. *Nat. Protocols* **2013**, *8*, 2392-2403.
36. Dreyer, D. R.; Park, S.; Bielawski, C. W.; Ruoff, R. S., The Chemistry of Graphene Oxide. *Chem. Soc. Rev.* **2010**, *39*, 228-240.
37. Potts, J. R.; Dreyer, D. R.; Bielawski, C. W.; Ruoff, R. S., Graphene-Based Polymer Nanocomposites. *Polymer* **2011**, *52*, 5-25.
38. Lotfi, Z.; Mousavi, H. Z.; Sajjadi, S. M., Amino-Terminated Hyper-Branched Polyamidoamine Polymer Grafted Magnetic Graphene Oxide Nanosheets as an Efficient Sorbent for the Extraction of Selective Serotonin Reuptake Inhibitors from Plasma Samples. *Anal. Methods* **2017**, *9*, 4504-4513.
39. Joshi, R. K.; Carbone, P.; Wang, F. C.; Kravets, V. G.; Su, Y.; Grigorieva, I. V.; Wu, H. A.; Geim, A. K.; Nair, R. R., Precise and Ultrafast Molecular Sieving through Graphene Oxide Membranes. *Science* **2014**, *343*, 752-754.
40. Kumar, R.; Mamlouk, M.; Scott, K., Sulfonated Polyether Ether Ketone - Sulfonated Graphene Oxide Composite Membranes for Polymer Electrolyte Fuel Cells. *RSC Adv.* **2014**, *4*, 617-623.
41. Wu, C.; Huang, X.; Wang, G.; Wu, X.; Yang, K.; Li, S.; Jiang, P., Hyperbranched-Polymer Functionalization of Graphene Sheets for Enhanced Mechanical and Dielectric Properties of Polyurethane Composites. *J. Mater. Chem.* **2012**, *22*, 7010-7019.
42. Nair, R. R.; Wu, H. A.; Jayaram, P. N.; Grigorieva, I. V.; Geim, A. K., Unimpeded Permeation of Water through Helium-Leak-Tight Graphene-Based Membranes. *Science* **2012**, *335*, 442-444.
43. Abraham, J., et al., Tunable Sieving of Ions Using Graphene Oxide Membranes. *Nat. Nanotechnol.* **2017**, *12*, 546.

44. Shau, S. M.; Juang, T. Y.; Lin, H. S.; Huang, C. L.; Hsieh, C. F.; Wu, J. Y.; Jeng, R. J., Individual Graphene Oxide Platelets through Direct Molecular Exfoliation with Globular Amphiphilic Hyperbranched Polymers. *Polym Chem-Uk* **2012**, *3*, 1249-1259.
45. Rissanou, A. N.; Bačová, P.; Harmandaris, V., Properties of Nanographene in Polymer Nanocomposites through All-Atom Simulations: Shape Fluctuations and Rippling. *Comput. Mater. Sci.* **2020**, *172*, 109330.
46. Karatasos, K.; Kritikos, G., A Microscopic View of Graphene-Oxide/Poly(Acrylic Acid) Physical Hydrogels: Effects of Polymer Charge and Graphene Oxide Loading. *Soft Matter* **2018**, *14*, 614-627
47. Kritikos, G.; Pant, R.; Sengupta, S.; Karatasos, K.; Venkatnathan, A.; Lyulin, A. V., Nanostructure and Dynamics of Humidified Nafion/Graphene-Oxide Composites Via Molecular Dynamics Simulations. *J. Phys. Chem. C* **2018**, *122*, 22864-22875.
48. Karatasos, K.; Kritikos, G., Characterization of a Graphene Oxide/Poly(Acrylic Acid) Nanocomposite by Means of Molecular Dynamics Simulations. *RSC Adv.* **2016**, *6*, 109267.
49. Rissanou, A. N.; Harmandaris, V., A Molecular Dynamics Study of Polymer/Graphene Nanocomposites. *Macromol. Symp.* **2013**, *331-332*, 43-49.
50. Karatasos, K., Graphene/Hyperbranched Polymer Nanocomposites: Insight from Molecular Dynamics Simulations. *Macromolecules* **2014**, *47*, 8833-8845.
51. Kumar, A.; Sharma, K.; Dixit, A. R., A Review on the Mechanical and Thermal Properties of Graphene and Graphene-Based Polymer Nanocomposites: Understanding of Modelling and Md Simulation. *Mol. Sim.* **2020**, *46*, 136-154.
52. Cakara, D.; Kleimann, J.; Borkovec, M., Microscopic Protonation Equilibria of Poly(Amidoamine) Dendrimers from Macroscopic Titrations. *Macromolecules* **2003**, *36*, 4201-4207.
53. Xiao, W. D.; Yan, B.; Zeng, H. B.; Liu, Q. X., Dendrimer Functionalized Graphene Oxide for Selenium Removal. *Carbon* **2016**, *105*, 655-664.
54. Vusa, C. S. R.; Manju, V.; Berchmans, S.; Arumugam, P., Electrochemical Amination of Graphene Using Nanosized Pamam Dendrimers for Sensing Applications. *RSC Adv.* **2016**, *6*, 33409-33418.
55. Piao, Y. Z.; Wu, T. F.; Chen, B. Q., One-Step Synthesis of Graphene Oxide-Polyamidoamine Dendrimer Nanocomposite Hydrogels by Self-Assembly. *Ind. Eng. Chem. Res.* **2016**, *55*, 6113-6121.
56. Liu, M.; Hou, Z.; Huang, B.; Gou, L.; Zhang, P., The Preparation, Characterization, and Properties of Silver Nanoparticle Reinforced Reduced Graphene Oxide–Poly(Amidoamine) Nanocomposites. *J. Appl. Polym. Sci.* **2017**, *134*, 45172.
57. Guo, R. B.; Han, W. W.; Mo, Z. L.; Li, L.; Feng, C., Molecular Dynamics Study on the Microstructure of Dendrimers/Graphite Composites. *J. Mater. Res.* **2012**, *27*, 1124-1130.
58. Vasumathi, V.; Pramanik, D.; Sood, A. K.; Maiti, P. K., Structure of a Carbon Nanotube-Dendrimer Composite. *Soft Matter* **2013**, *9*, 1372-1380.
59. Pramanik, D.; Maiti, P. K., Dendrimer Assisted Dispersion of Carbon Nanotubes: A Molecular Dynamics Study. *Soft Matter* **2016**, *12*, 8512-8520.
60. Lerf, A.; He, H.; Forster, M.; Klinowski, J., Structure of Graphite Oxide Revisited. *J. Phys. Chem. B* **1998**, *102*, 4477-4482.
61. Shih, C. J.; Lin, S. C.; Sharma, R.; Strano, M. S.; Blankschtein, D., Understanding the Ph-Dependent Behavior of Graphene Oxide Aqueous Solutions: A Comparative Experimental and Molecular Dynamics Simulation Study. *Langmuir* **2012**, *28*, 235-241.
62. Konkena, B.; Vasudevan, S., Understanding Aqueous Dispersibility of Graphene Oxide and Reduced Graphene Oxide through Pka Measurements. *J. Phys. Chem. Lett.* **2012**, *3*, 867-872.
63. Jorgensen, W. L.; Maxwell, D. S.; TiradoRives, J., Development and Testing of the Opls All-Atom Force Field on Conformational Energetics and Properties of Organic Liquids. *J Am Chem Soc* **1996**, *118*, 11225-11236.
64. Tang, H.; Zhao, Y.; Yang, X. N.; Liu, D. M.; Shan, S. J.; Cui, F. Y.; Xing, B. S., Understanding the Ph-Dependent Adsorption of Ionizable Compounds on Graphene Oxide Using Molecular Dynamics Simulations. *Environ. Sci. Nano* **2017**, *4*, 1935-1943.
65. Tang, H.; Liu, D.; Zhao, Y.; Yang, X.; Lu, J.; Cui, F., Molecular Dynamics Study of the Aggregation Process of Graphene Oxide in Water. *J. Phys. Chem. C* **2015**, *119*, 26712-26718.
66. Wei, N.; Lv, C.; Xu, Z., Wetting of Graphene Oxide: A Molecular Dynamics Study. *Langmuir* **2014**, *30*, 3572-3578.
67. Tanis, I.; Karatasos, K., Molecular Dynamics Simulations of Polyamidoamine Dendrimers and Their Complexes with Linear Poly(Ethyleneoxide) at Different Ph Conditions: Static Properties and Hydrogen Bonding. *Phys. Chem. Chem. Phys.* **2009**, *11*, 10017–10028.
68. W. L. Jorgensen; J. Chandrasekhar; J.D. Madura; R.W. Impey; Klein, M., Comparison of Simple Potential Functions for Simulating Liquid Water. *J. Chem. Phys.* **1983**, *79*, 926

69. Maiti, P. K.; Cagin, T.; Lin, S. T.; Goddard, W. A., Effect of Solvent and Ph on the Structure of Pamam Dendrimers. *Macromolecules* **2005**, *38*, 979-991.
70. Li, D.; Muller, M. B.; Gilje, S.; Kaner, R. B.; Wallace, G. G., Processable Aqueous Dispersions of Graphene Nanosheets. *Nat. Nanotechnol.* **2008**, *3*, 101-105.
71. Wang, G.; Yang, J.; Xinglong, J.; Wang, B.; HaoYao, J., Facile Synthesis and Characterization of Graphene Nanosheets. *J. Phys. Chem. C* **2008**, *112*.
72. Zhou, H.; Cheng, C.; Qin, H.; Ma, L.; He, C.; Nie, S.; Zhang, X.; Fu, Q.; Zhao, C., Self-Assembled 3d Biocompatible and Bioactive Layer at the Macro-Interface Via Graphene-Based Supermolecules. *Polym Chem-Uk* **2014**, *5*, 3563.
73. Martínez, L.; Andrade, R.; Birgin, E. G.; Martínez, J. M., Packmol: A Package for Building Initial Configurations for Molecular Dynamics Simulations. *J. Comput. Chem.* **2009**, *30*, 2157-2164.
74. Feller, S. E.; Zhang, Y.; Pastor, R. W.; Brooks, B. R., Constant Pressure Molecular Dynamics Simulation: The Langevin Piston Method. *J. Chem. Phys.* **1995**, *103*, 4613-4621.
75. Darden, T.; Perera, L.; Li, L.; Pedersen, L., New Tricks for Modelers from the Crystallography Toolkit: The Particle Mesh Ewald Algorithm and Its Use in Nucleic Acid Simulations. *Structure* **1999**, *7*, R55-R60.
76. Phillips, J.; Braun, R.; Wang, W.; Gumbart , J.; Tajkhorshid, E.; Villa, E.; Chipot, C.; Skeel, R.; Kale, L.; Schulten, K., Scalable Molecular Dynamics with Namd. *J. Comput. Chem.* **2005**, *26*, 1781–1782.
77. Rudnick, J.; Gaspari, G., The Aspherity of Random Walks. *J. Phys. A: Math. Gen.* **1986**, *19*, L191-L193.
78. Maiti, P. K.; Bagchi, B., Diffusion of Flexible, Charged, Nanoscopic Molecules in Solution: Size and Ph Dependence for Pamam Dendrimer. *J. Chem. Phys.* **2009**, *131*.
79. Carbone, P.; Muller-Plathe, F., Molecular Dynamics Simulations of Polyaminoamide (Pamam) Dendrimer Aggregates: Molecular Shape, Hydrogen Bonds and Local Dynamics. *Soft Matter* **2009**, *5*, 2638-2647.
80. Prosa, T. J.; Bauer, B. J.; Amis, E. J., From Stars to Spheres: A Saxs Analysis of Dilute Dendrimer Solutions. *Macromolecules* **2001**, *34*, 4897-4906.
81. Karatasos, K.; Adolf, D. B.; Davies, G. R., Statics and Dynamics of Model Dendrimers as Studied by Molecular Dynamics Simulations. *J. Chem. Phys.* **2001**, *115*, 5310-5318.
82. Maiti, P. K.; Cagin, T.; Wang, B.; Goddard III, W. A., Structure of Pamam Dendrimers: Generations 1 through 11. *Macromolecules* **2004**, *37*, 6236.
83. Gosika, M.; Maiti, P. K., Ph and Generation Dependent Morphologies of Pamam Dendrimers on a Graphene Substrate. *Soft Matter* **2018**, *14*, 1925-1938.
84. Gosika, M.; Sen, S.; Kundagrami, A.; Maiti, P. K., Understanding the Thermodynamics of the Binding of Pamam Dendrimers to Graphene: A Combined Analytical and Simulation Study. *Langmuir* **2019**, *35*, 9219-9232.
85. Zallen, R., *The Physics of Amorphous Solids*; Wiley, 1998.
86. Lerf, A.; Buchsteiner, A.; Pieper, J.; Schöttl, S.; Dekany, I.; Szabo, T.; Boehm, H. P., Hydration Behavior and Dynamics of Water Molecules in Graphite Oxide. *J. Phys. Chem. Solids* **2006**, *67*, 1106-1110.
87. Buchsteiner, A.; Lerf, A.; Pieper, J., Water Dynamics in Graphite Oxide Investigated with Neutron Scattering. *J. Phys. Chem B.* **2006**, *110*, 22328-22338.
88. Rezania, B.; Severin, N.; Talyzin, A. V.; Rabe, J. P., Hydration of Bilayered Graphene Oxide. *Nano Lett.* **2014**, *14*, 3993-3998.
89. Devanathan, R.; Chase-Woods, D.; Shin, Y.; Gotthold, D. W., Molecular Dynamics Simulations Reveal That Water Diffusion between Graphene Oxide Layers Is Slow. *Sci Rep-Uk* **2016**, *6*.
90. Raghav, N.; Chakraborty, S.; Maiti, P. K., Molecular Mechanism of Water Permeation in a Helium Impermeable Graphene and Graphene Oxide Membrane. *Phys. Chem. Chem. Phys.* **2015**, *17*, 20557-20562.
91. Brocorens, P.; Lazzaroni, R.; Bredas, J. L., The Conformation of Amine- and Amide-Terminated Poly(Propylene Imine) Dendrimers as Investigated by Molecular Simulation Methods. *J. Phys. Chem. B* **2005**, *109*, 19897-19907.
92. Chiessi, E.; Cavalieri, F.; Paradossi, G., Water and Polymer Dynamics in Chemically Cross-Linked Hydrogels of Poly(Vinyl Alcohol): A Molecular Dynamics Simulation Study. *J. Phys. Chem. B* **2007**, *111*, 2820-2827.
93. Tanis, I.; Tragoudaras, D.; Karatasos, K.; Anastasiadis, S. H., Molecular Dynamics Simulations of a Hyperbranched Poly(Ester Amide): Statics, Dynamics, and Hydrogen Bonding. *J. Phys. Chem. B* **2009**, *113*, 5356-5368.
94. Rapaport, D. C., Hydrogen Bonds in Water -- Network Organization and Lifetimes. *Mol. Phys.* **1983**, *50*, 1151 - 1162.

95. Fan, Y.-C.; Fang, T.-H.; Huang, C.-C.; Chen, T.-H., Atomic Simulation of Wrinkling and Deformation in Curved Graphene Nanoribbons under Boundary Confinement. *Mater. Des.* **2016**, *89*, 470-475.
96. Kritikos, G.; Karatasos, K., Temperature Dependence of Dynamic and Mechanical Properties in Poly(Acrylic Acid)/Graphene Oxide Nanocomposites. *Mater. Today Commun.* **2017**, *13*, 359-366.
97. Zhu, Y.; Murali, S.; Cai, W.; Li, X.; Suk, J. W.; Potts, J. R.; Ruoff, R. S., Graphene and Graphene Oxide: Synthesis, Properties, and Applications. *Adv. Mater.* **2010**, *22*, 3906-3924.
98. Geffrey, G. A.; Saenger, W., *Hydrogen Bonding in Biological Structures*; Springer-Verlag: Heilderberg, 1991.
99. Sheu, S.-Y.; Yang, D.-Y.; Selzle, H. L.; Schlag, E. W., Energetics of Hydrogen Bonds in Peptides. *Proc Natl Acad Sci U S A* **2003**, *100*, 12683-12687.

## "TOC Graphic"